

CHARACTERISATION OF TWO WASTES FROM A COPPER SMELTING ELECTRIC ARC FURNACE AND DIAGNOSE FOR VALORIZATION

S.M Pérez-Moreno¹, M.J. Gázquez¹, G. Ríos², I. Ruiz-Oria² and J.P. Bolívar^{1}*

¹*Department of Applied Physics, University of Huelva, Huelva, Spain*

²*Atlantic Copper S.L.U, Huelva, Spain.*

**Corresponding author: E-mail: bolivar@uhu.es, Tel.: +34-959219793, Fax: +34-959219777*

Abstract

The present study was conducted using two forms of waste from an electric furnace in the copper smelting industry in order to study their elemental composition, granulometry, mineralogy, microscopic morphology, etc. as a step towards their valorisation for use in the manufacturing of commercial products.

Several techniques were used in this study: X-ray fluorescence, ICP-MS, X-ray diffraction, laser granulometry, thermogravimetric analysis, microstructural analysis and leaching tests.

The results demonstrated that these wastes are formed of agglomerates of very fine particles. They are mainly composed of Zn (20%–40%) and Pb (5%–10%). Their crystalline fraction is mostly zincite (ZnO), among others. They also contain various sulphates (FeSO₄, CaSO₄) and species of carbonates (CaCO₃, PbCO₃). According to leaching tests, these are classified as hazardous residues, and their elimination in a controlled repository therefore involves very high costs. Taking into account this fact and their high concentrations of Pb and Zn, their valorisation through the recovery of these metals may be possible.

Keywords: *Copper smelting, Electric furnace dust, Desulphurisation, Waste characterisation waste, Valorisation.*

1. Introduction

Copper is one of the oldest metals ever used, and has been one of the most significant materials in the development of many civilizations. Since it is a ductile metal with very high thermal and electrical conductivity, it is mainly used as electrical conductor, and to a lesser extent as a heat conductor [1].

Copper occurs in nature predominantly as chalcopyrite (CuFeS₂), and is almost always accompanied by the iron sulphides pyrite (FeS₂) and pyrrhotite (FeS). Copper sulphide ores also can contain other metal sulphides such as molybdenite (MoS₂), sphalerite (ZnS) and galena (PbS). Copper is generally found in very low percentages in nature (0.5%–2%), but its ore can be ground up and concentrated to around 25% to 30 % using froth flotation.

The pyrometallurgical process for obtaining very pure metal begins by mixing the copper concentrate with a SiO₂ flux and introducing it into the flash furnace (FF), where the fusion process takes place. Most sulphur is converted to SO₂ and sent to the acid plant to be converted to sulphuric acid. The oxidised iron combines with the silica, added initially to the concentrate, to form a fayalite slag (2FeO·SiO₂). The remaining melt phase (Cu, Fe, and other metals) forms a liquid copper matte containing 50%–70% of Cu (Figure 1).

The matte (mainly Cu₂S and FeS) is separated from the slag and fed into the converting furnace (CF), where the copper is separated from the left-over sulphur, iron and other metals not eliminated in the FF. Consequently, SO₂ and slag are produced again. The conversion furnace yields a product called “blister copper”, which has a copper content of approximately 99%. The small amounts of sulphur and iron still remaining in the blister copper are removed by further oxidation in a fire-refining furnace. The fire-refined copper is cast into anodes that go to the electrolytic cell to be refined to 99.99% copper in the cathodes [2].

The slags produced in the FF and CF are treated in an electric arc furnace (EAF) to recover copper from matte containing 1.5% and 5% respectively, leaving a final slag with a content of below 1% Cu. The remaining slag is then cooled and granulated with water to make an industrial product which is used in many applications in civil engineering and as an abrasive [3, 4].

The main emissions from the smelting industrial process are gas flows and liquid streams [5, 6]. Directive 2010/75/EU of the European Parliament [7] and the Industrial Emissions Directive (IED) is the main EU instrument regulating pollutant emissions from industrial installations. The proposed goals are achieved through emission limitations that require the use of technology-based controls.

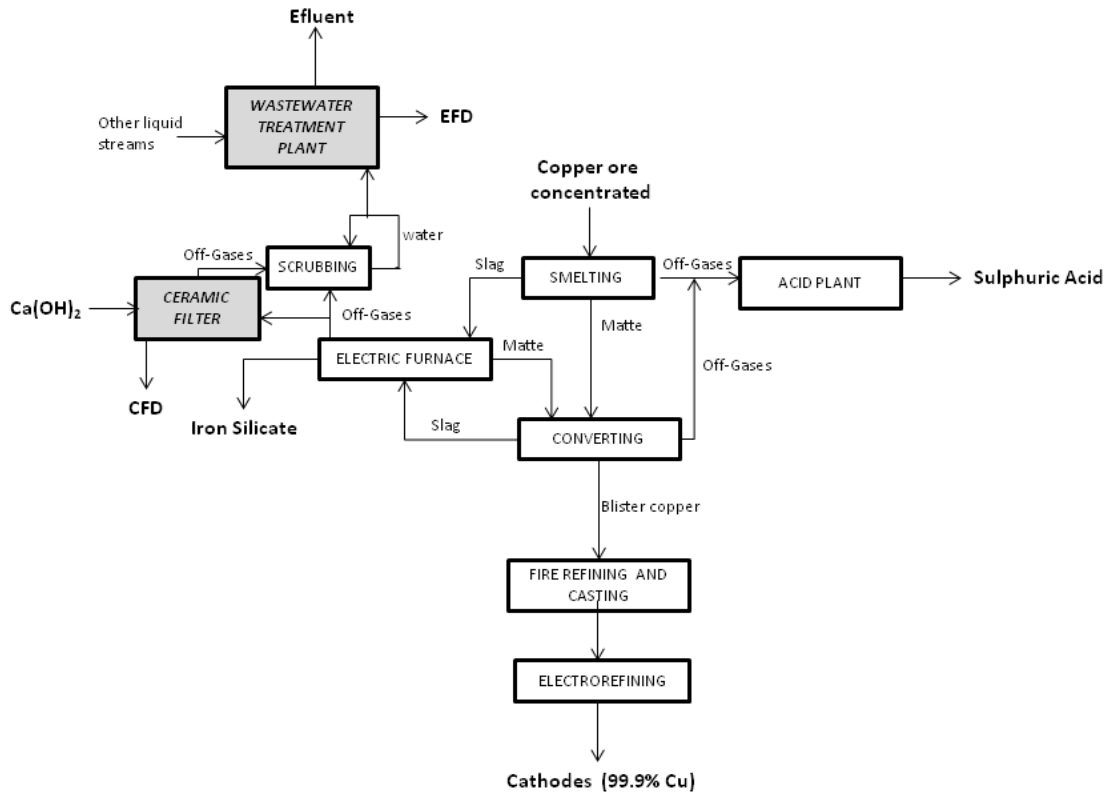


Figure 1. Overview of material flows and processes

The characteristics of the gases dictate the type of control technology, which in turn determines the kind of by-products produced [8]. Stronger streams with high SO₂ concentration are used to generate sulphuric acid. This is the most widely used control technology in order to achieve economical operation and compliance with pollution limitations. However, weak gas streams, with a SO₂ concentration of less than 4% by volume, constitute a more difficult and costly problem.

Scrubbing with water is one of the methods used to treat streams with low SO₂ concentration by Atlantic Copper S.L.U., a copper smelting located in Huelva, southwest Spain. In practice, this scrubbing system (wet treatment) is used to treat the off-gases from the electric arc furnace. This method helps to remove gases and particles which are trapped in the water. In order to avoid a high concentration of impurities in the water, some of this water is treated in a wastewater treatment plant (WTP), along with other liquid streams from other plants within the industry. The EAF liquid stream forms about 80% of the total volume treated at the WTP, where different reagents are added (NaOH, coagulants, flocculants, etc.). This treatment gives rise to a solid waste (EFD), containing about 60% water, and classified as hazardous material according to the Waste European Directive. About 2500 t/y of EFD are currently produced, and these are subjected to an inertisation process before their elimination in a controlled hazardous waste landfill, located 70 km from the smelting factory.

In recent years, increases in copper production and degradation of the quality of copper ore have resulted in higher amounts of particles and gases from this process. In addition, environmental regulations have become stricter. Due to environmental concerns, the amount of solid waste disposed of is required to be reduced, driving a search for new alternatives in the treatment of gases and particles to diminish the production of final residue [9].

The copper smelting located in Huelva suggests new stream treatment strategies, particularly in the off-gases from the EAF. A new technology is now being studied which consists of flue-gas desulphurisation in a ceramic sleeve filter (CF) using micronised calcium hydroxide. This operation is based on the adsorption of gas pollutants onto fine-grained solid particles of Ca(OH)₂, which is introduced in the gas stream and is finally collected onto a CF. A pilot plant has been installed in the factory for this purpose. The new treatment gives a final dry solid waste (CFD). Furthermore, this will mean a significant reduction in the consumption of water and the volume of discharge into the environment.

In view of these facts, this study aims to examine the physico-chemical characterisation of these two waste streams (EFD and CFD) generated in the two desulphurisation treatments from EAF off-gases, in order to acquire basic information as an essential step towards the pursuit of realistic applications or treatments for these wastes.

2. Materials and Methods

2.1 Material

The samples used in this study, EFD and CFD, were collected from a copper smelting plant in Huelva, south-western Spain. Five sampling campaigns were organised over a period of one month in October 2015. After collection, the samples were dried at 60°C until a constant weight was reached.

2.2 Methods for physical and chemical characterisation

2.2.1 Granulometry

The particle size range of the samples was determined using a modular analyser, the Mastersizer 2000, with He-Ne laser diffraction technology at a wavelength of 632.8 nm. A representative amount of each sample was placed in water and subjected to ultrasound for 10 min, followed by magnetic stirring for approximately 30 min.

2.2.2 Mineralogy

X-ray diffraction analysis was performed using a Panalytical X'Pert Pro diffractometer, equipped with a Cu X-ray source and an X'celerator detector, operating under the following conditions: voltage 40 kV; current 40 mA; range 5–70 deg 2 θ ; step size 0.017 deg 2 θ ; time per step 50.165 sec; divergence slit fixed, angle 0.5°. The crystalline mineral phases were identified using an X'Pert HighScore Plus with the PDF-4 Minerals 2013 ICDD database. The quantities of the crystalline minerals were determined using the Rietveld method. Corundum was used as an internal standard to determine the amount of amorphous material.

2.2.3 Chemical analysis

The major elements were measured using an X-ray fluorescence Panalytical spectrometer (AXIOS model) with an Rh tube and two detectors (scintillation and flow). Prior to the analysis, the samples were prepared as pressed tablets of 40 mm diameter and 25 mm thickness.

The trace elements were analysed using two measurement techniques: ICP-MS (Perkin Elmer Sciex ELAN 9000), and ICP-OES (Varian 735ES). Prior to analysis, samples were digested by combining four acids (hydrochloric, nitric, perchloric and hydrofluoric) and some aliquots were dissolved by fusion with sodium peroxide.

2.2.4 Thermogravimetric analysis

In the thermal gravimetric analysis and differential thermal analysis a TG-851E 11 SDTA Mettler thermobalance was employed, coupled to a Pfeiffer ThermoStar mass spectrometer. The operating conditions used were 25°C–1000°C with a heating rate of 10°C min⁻¹ and an inert atmosphere of N₂ with a flow of 50 ml min⁻¹.

2.2.5 Scanning electron microscopy

The morphology and microstructure of the samples were studied using an environmental scanning electron microscope (QUANTA Fei-200). This equipment also enabled a multi-elemental semi-quantitative analysis using energy dispersive spectroscopy (EDS). Following this, a mineralogy database [10] was used to determine the mineralogical composition.

The spatial distribution of several elements was obtained using a scanning electron microprobe (EPMA) JEOL JXA-8200 model with four wavelength-dispersive X-ray spectrometers and energy-dispersive X-ray spectrometers (EDS).

2.2.6 Leaching test

Two leaching tests were applied: the toxicity characteristic leaching procedure (TCLP) from USEPA [11] and the UNE-EN 12457-4 test [12] from Directive 1999/31/CE.

USEPA test method 1311 was adopted in this experiment. The extraction fluid used was 5.7 mL of glacial acetic acid diluted in water to a volume of 1 L. The pH of the extraction fluid measured with a calibrated pH meter was 2.88 ± 0.05. A liquid/solid ratio of 20:1 and 16 h extraction time was used for the TCLP tests. The agitation apparatus, rotation speeds, extraction vessels and filtration devices were as recommended in the USEPA 1311 method.

The European Commission regulates disposal waste in landfill through Directive 1999/31/CE, and the waste acceptance criteria are established for each class of landfill in Directive UNE-EN 12457-4. The leaching tests set out in this CE Directive were adopted in our experiments. The extraction fluid used was distilled water at a liquid/solid ratio of 10 L/kg \pm 2%. The agitation apparatus, rotation speeds, extraction vessels, filtration devices and extraction time (24 h) were as recommended in this Directive.

3. Results and discussion

3.1 Granulometry

The particle size distribution (% volume) of samples obtained after granulometry analysis is summarised in Table 1. The EFD is characterised by a high concentration of silt (62%; 4–62 microns), a moderate concentration of sand (24%; 62–2000 microns) and also contains a certain proportion of clay (14.1%; < 4 microns). This grain size distribution is a well-defined multimodal distribution, in which the maximum volumes of particles are of 0.6, 7 and 60 microns diameter respectively (Figure 2).

In the same way, the CFD has a high concentration of silt (73%; 4–62 microns), a moderate concentration of clay (18.1%; < 4 microns), but contains sand at a lower proportion (9.0%; 62–2000 microns). CFD also presents a multimodal distribution. The maximum volumes of particles are also of 0.6, 7 and 60 microns in diameter.

Size (μm)	Type	EFD (%)		CFD (%)	
		Average concentration	Global	Average concentration	Global
<4	Clay	14.1 \pm 3.2	14.1 \pm 3.2	18.1 \pm 4.1	18.1 \pm 4.1
4-8	Silt	17.1 \pm 1.8	61.8 \pm 3.8	26.6 \pm 1.8	72.8 \pm 3.6
8-16		15.6 \pm 2.9		23.5 \pm 2.9	
16-32		13.3 \pm 1.2		12.8 \pm 0.9	
32-62		15.8 \pm 1.1		9.87 \pm 0.78	
62-125		14.9 \pm 2.1		6.77 \pm 1.81	
125-250	Sand	7.49 \pm 1.67	24.1 \pm 2.7	2.07 \pm 0.88	9.05 \pm 2.02
250-500		1.62 \pm 0.56		0.20 \pm 0.04	
500-1000		0.08 \pm 0.02		-	
1000-2000		-		-	

Table 1. Average grain size distribution (%V) of the studied samples. Standard uncertainty (1σ) has been calculated as the standard deviation of the mean, $\sigma = Sx/(n)^{1/2}$

A multimodal distribution may arise from a process involving the breakup of large particles, multiple sources of particles or variable growth mechanisms in the system. There are few studies reporting on the particle formation in an EAF [13, 14]. The dust from the EAF covers a wide range of sizes, and to simplify the survey of the morphologies, two categories of particle were distinguished: large particles of a few dozen to a few thousand micrometres, and finer particles of lower than 20 μm .

It is possible that the clay fractions may be generated due to the breakup of large particles; the other fractions may arise from the later process to which the dust is subjected in each case. According to the wet desulphurisation treatment in which EDF is generated, large particles may arise from other streams that are treated in the WTP. On the other hand, in the new dry desulphurisation treatment in which CFD is formed, large particles may be generated by the reagent added. These particles were studied using scanning electron microscopy (Section 3.5).

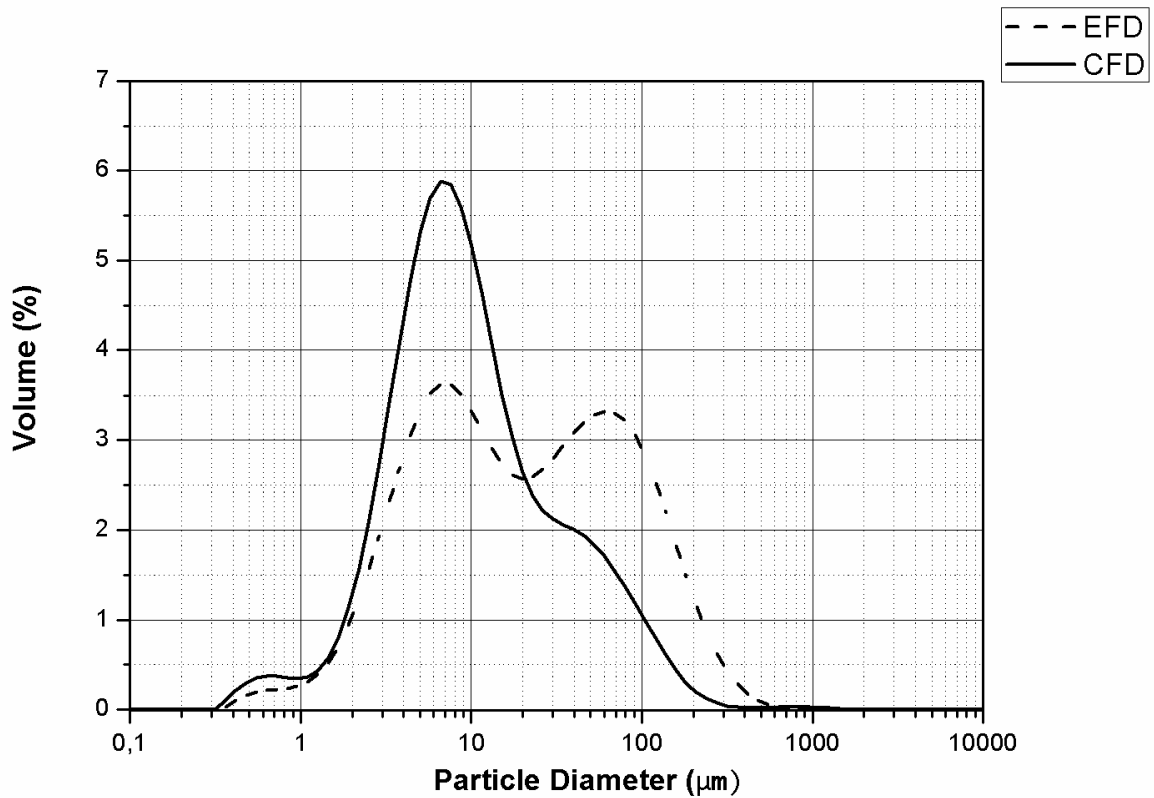


Figure 2. Particle size distribution (%V) of samples.

3.2 Mineralogy

Fig. 3 shows the X-ray diffraction powder spectrum of the EFD and CFD. Zincite (ZnO), magnetite (Fe₃O₄), ramsdellite (MnO), quartz (SiO₂) and cristobalite (SiO₂) are the most significant minerals present in the EFD. Their quantification is presented in Table 2. The sample is characterised by a high quantity of amorphous phase (62.6%) and the mineral zincite (26%) as the main crystalline phase.

	EFD (%)	CFD (%)
Zincite (ZnO)	26.0	9.3
Portlandite (Ca(OH) ₂)	n.d	13.9
Anglesite (PbSO ₄)	n.d	3.3
Magnetite (Fe ₃ O ₄)	7.5	1.6
Goethite (FeO(OH))	n.d	0.8
Ramsdellite (MnO)	2.4	n.d
Calcite (CaCO ₃)	n.d	0.8
Quartz (SiO ₂)	0.5	n.d
Cristobalite (SiO ₂)	1.0	n.d
Amorphous	62.6	70.2

Note: n.d. = not detected; amorphous includes X-ray amorphous material and unidentified phases.

Table 2. Minerals identified and their amounts (wt %)

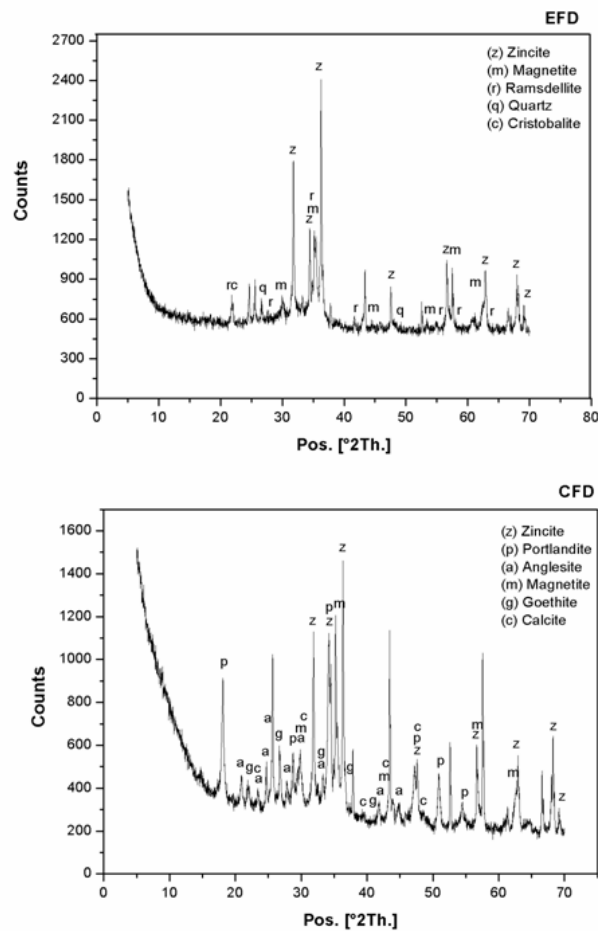


Figure 3. X-ray diffraction (XRD) pattern of EFD and CFD

The CFD contained zincite (ZnO), portlandite (Ca(OH)₂), anglesite (PbSO₄), magnetite (Fe₃O₄), goethite (FeO(OH)) and calcite (CaCO₃) as mineral phases. The quantities of the crystalline minerals are indicated in Table 2. The CFD is also characterised by a high proportion of amorphous phase (> 70%) and contains portlandite (14%) and zincite (9.3%) as the main crystal phases. The portlandite comes from the unreacted residual chemical agent employed in the neutralisation of the electric furnace gas stream (Ca(OH)₂), which is collected in the CF. Otherwise, the existence of forced air ventilation system helps the Ca(OH)₂ to react with the CO₂ in the air, producing calcite in the following reaction [15]:



Some of the identified mineral phases, zincite (ZnO) and magnetite (Fe₃O₄), were detected in both samples. This was as expected, since these have the same origin in the electrical furnace.

3.3 Chemical analysis

The concentrations of the major elements of the samples studied are shown in Table 3.

Element	EFD (%)	CFD (%)	Undisturbed soil (*)
Al	0.34 ± 0.01	0.18 ± 0.01	8.15 ± 0.40
As	2.79 ± 0.63	1.20 ± 0.03	(5.7 ± 1.2) · 10 ⁻⁴
Bi	0.28 ± 0.01	0.17 ± 0.04	(2.30 ± 0.3) · 10 ⁻⁵
Ca	0.57 ± 0.11	23.2 ± 2.2	2.6 ± 0.1
Cd	0.24 ± 0.03	0.15 ± 0.01	(0.6 ± 0.2) · 10 ⁻⁵
Cl	0.11 ± 0.01	0.09 ± 0.01	(3.7 ± 3.8) · 10 ⁻²
Cu	3.62 ± 0.18	1.75 ± 0.14	(2.7 ± 0.2) · 10 ⁻³
Fe	14.1 ± 1.9	2.60 ± 0.19	3.9 ± 0.4
K	0.10 ± 0.02	0.48 ± 0.12	2.3 ± 0.2
Mg	0.29 ± 0.02	0.16 ± 0.01	1.5 ± 0.2
Mo	0.16 ± 0.01	0.10 ± 0.01	(0.6 ± 0.3) · 10 ⁻⁴
Na	0.26 ± 0.01	0.17 ± 0.01	2.42 ± 0.36
O	17.8 ± 1.0	25.4 ± 2.4	-
P	0.25 ± 0.02	0.07 ± 0.02	0.07 ± 0.01
Pb	7.12 ± 1.89	4.45 ± 1.15	(1.7 ± 0.1) · 10 ⁻³
S	0.43 ± 0.07	4.94 ± 0.01	(6.2 ± 0.3) · 10 ⁻²
Sb	0.53 ± 0.04	0.30 ± 0.02	(7.5 ± 1.1) · 10 ⁻⁵
Si	2.32 ± 0.36	0.99 ± 0.07	31 ± 1
Sn	0.15 ± 0.04	0.09 ± 0.04	(2.2 ± 0.2) · 10 ⁻⁴
Zn	41.4 ± 0.3	22.3 ± 4.6	(7.5 ± 0.9) · 10 ⁻³
LOI	7.35 ± 0.21	11.5 ± 1.2	-

Table 3. Concentrations (%) of major elements in samples. Standard uncertainty (1σ) has been calculated as standard deviation of the mean as $\sigma = Sx/(n)^{1/2}$. (*)Worldwide average concentrations taken from Rudnick and GaO (2003) and Hu and Gao (2008).

The EFD contained Zn (41.4%), O (17.8%), Fe (14.1%) and Pb (7.12%) as the major elements. Also it has Cu (3.62%), As (2.79%) and Si (2.32%), although in much lower proportions.

The CFD is characterised by its concentrations of O (25.4%), Ca (23.2%) and Zn (22.3%). In addition, S (4.94%), Pb (4.45%), Fe (2.60%), Cu (1.75%), As (1.20%) and Si (0.99%) are present in the sample, but at low proportions.

When the major element concentrations of the samples are compared between both wastes, the data are adapted to a linear equation (Fig. 4) with the exception of Fe, S, O, and Ca:

$$C_{\text{EFD}} = (-0.03 \pm 0.12) + (1.85 \pm 0.02) \cdot C_{\text{CFD}} \quad (R^2 = 0.998)$$

Thus the concentrations of the majority of the elements in the EFD are almost twice those of the CFD.

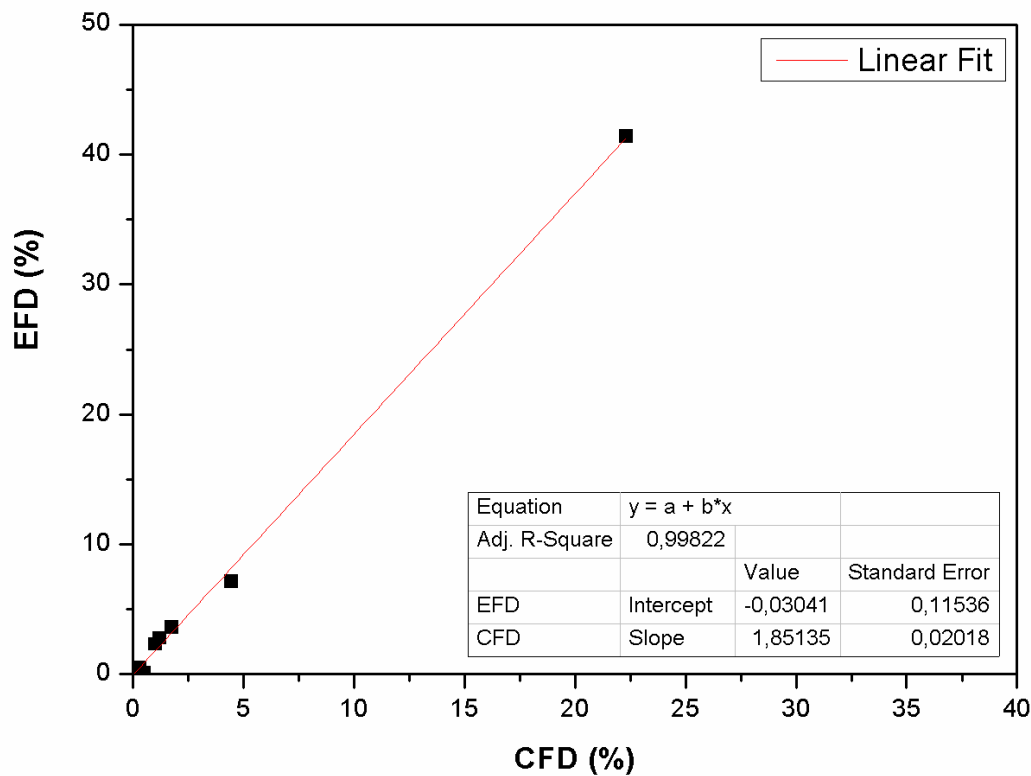


Figure 4. Comparison of the major elements in EFD and CFD.

The previous result confirms that both samples are of similar origin; however, this linear relation is not verified for Ca, O, S, Ca due to the following considerations:

Wet treatment (EFD): the gases and particulate matter from the EAF are treated in a scrubber with water, and the resulting dirty water is later managed in a WTP. Thus, the sulphur oxides contained in these gases are dissolved in water. For this reason, the solid material obtained after this process has a low concentration of sulphur (0.42%).

The high amount of iron in the EFD (14.1%), is generated by another water stream coming from slag granulation and going to the same WTP.

Dry treatment (CFD): the gases and particles from the EAF are treated in a CF with Ca(OH)_2 in order to neutralise the gas streams. This means that the resulting solid (CFD) has a very much higher Ca concentration (23.2%) than the EFD (0.6%).

When the results are compared with the average estimated composition of undisturbed soil (Table 3; Fig. 5) [16, 17], it is notable that most elements exceed the average concentrations for unperturbed soils. In practice, both Cd and Bi concentrations exceed the reference values by four orders of magnitude; As, Cu, Mo, Pb, Sb, Sn and Zn exceed the reference values by about three orders of magnitude; S exceeds the reference value by about 100 times; and Ca, Cl, Fe and P exceed the reference level by about 10 times. Only Al, K, Mg, Na and Si are below the reference values.

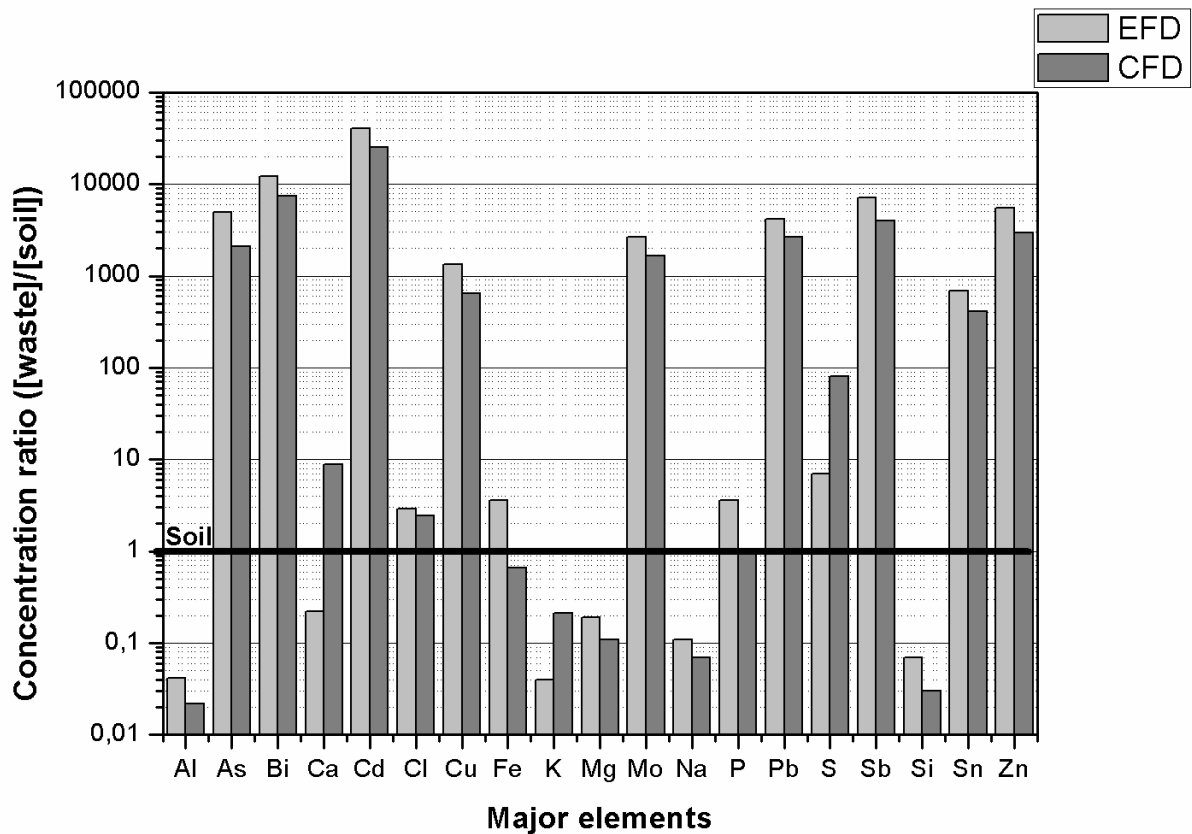


Figure 5. Comparison of the concentrations of the major elements with global estimated averages for undisturbed soil

Trace element concentrations for several elements are shown in Table 4. The EFD contains concentrations of Mn, Ni and In of higher than 100 ppm, while concentrations of Cr, Co, Zr, Sr and Se range from 80 to 50 ppm respectively. In addition, EFD presents concentrations of Ag, Tl, Ge and V which are detectable but lower than 40 ppm. Other elements, such as W, Te, Li, Re, Th and U, are at concentrations lower than 5 ppm.

The CFD contains Ba, Sr (> 100 ppm), Mn, Tl and In (50–80 ppm) as the main trace elements. It also contains Ni, Co, Se, Zr, Cr, Ag, Ge and V in concentrations lower than 50 ppm. Other elements, such as Li, W, Re, Te, U and Th, are at concentrations lower than 5 ppm.

Element	Detection limit (ppm)	EFD (ppm)	CFD (ppm)	Undisturbed soil (*)
Ag	0.05	34.8 ± 1.0	13.2 ± 1.4	0.053 ± 0.003
Ba	1.0	318 ± 19	160 ± 10	628 ± 83
Co	0.1	71.4 ± 3.8	30.6 ± 0.5	15 ± 1
Cr	0.5	76.3 ± 9.1	23.9 ± 7.8	74 ± 8
Ge	0.1	21.0 ± 10.2	12.9 ± 3.7	1.3 ± 0.1
In	0.1	120 ± 18	56.6 ± 3.8	0.066 ± 0.003
Li	0.5	2.74 ± 0.20	2.76 ± 0.07	41 ± 6
Mn	1.0	648 ± 52	74.0 ± 2.3	775 ± 78
Ni	0.5	138 ± 14	46.6 ± 3.0	34 ± 4
Re	0.001	2.03 ± 0.28	2.39 ± 0.42	0.0002
Se	0.1	55.9 ± 1.4	29.9 ± 1.2	0.09 ± 0.05
Sr	0.2	64.2 ± 15.2	114 ± 6	320 ± 46
Te	0.1	4.30 ± 0.41	1.73 ± 0.69	0.027 ± 0.003
Th	0.1	0.78 ± 0.08	0.36 ± 0.04	11 ± 1
Tl	0.05	31.2 ± 3.7	72.7 ± 3.9	0.53 ± 0.04
U	0.1	0.64 ± 0.17	1.53 ± 0.18	2.6 ± 0.1
V	1.0	13.3 ± 1.0	8.29 ± 0.97	106 ± 7
W	0.1	4.46 ± 1.83	2.55 ± 0.88	1.4 ± 0.1
Zr	1.0	68.0 ± 5.6	24.7 ± 1.5	193 ± 28

Table 4. Trace element concentrations (ppm) in samples. Standard uncertainty (1σ) has been calculated as standard deviation of the mean as $\sigma = Sx/(n)^{1/2}$. (*) Worldwide average concentrations taken from Rudnick and GaO (2003) and Hu and Gao (2008).

In the same way as for the major elements, when the trace elements of both samples are compared, the data are also a good fit to a linear equation with a slope of two (Fig. 6), with the exception of Mn, Sr and Tl:

$$C_{EFD} = (4.87 \pm 4.31) + (2.04 \pm 0.09) \cdot C_{CFD} \quad (R^2 = 0.969)$$

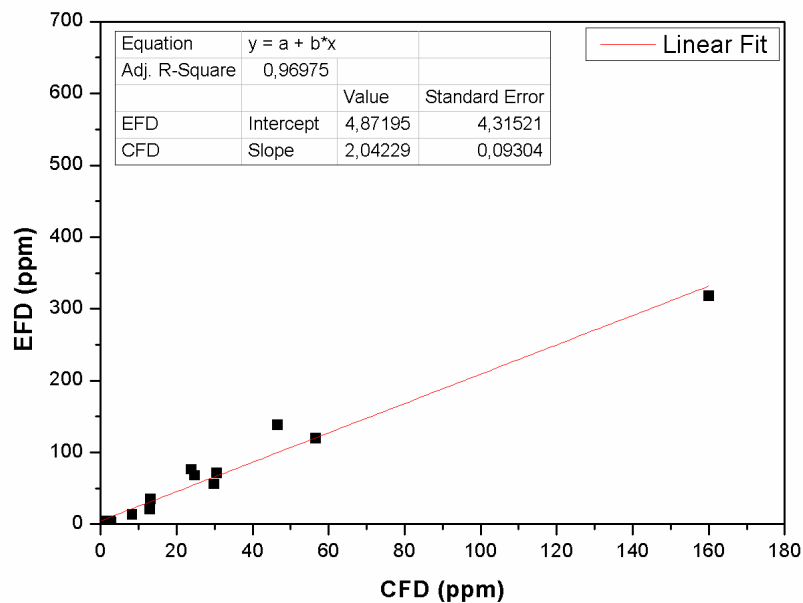


Figure 6. Comparison of trace elements of EFD and CFD.

When the results are compared with the average composition estimated for an undisturbed soil (Table 4; Fig. 7) [16, 17], it is notable that many elements exceed the estimated values. Specifically, Re exceeds the reference value by about four orders of magnitude; Ag, In and Se, exceed the reference value by about three orders of magnitude; Te and Tl exceed the reference value by about 100 times; and Co, Ge, Ni, and W exceed the reference value by about 10 times. Only Ba, Cr, Li, Mn, Sr, Th, U, V and Zr and Si are below the soil reference values.

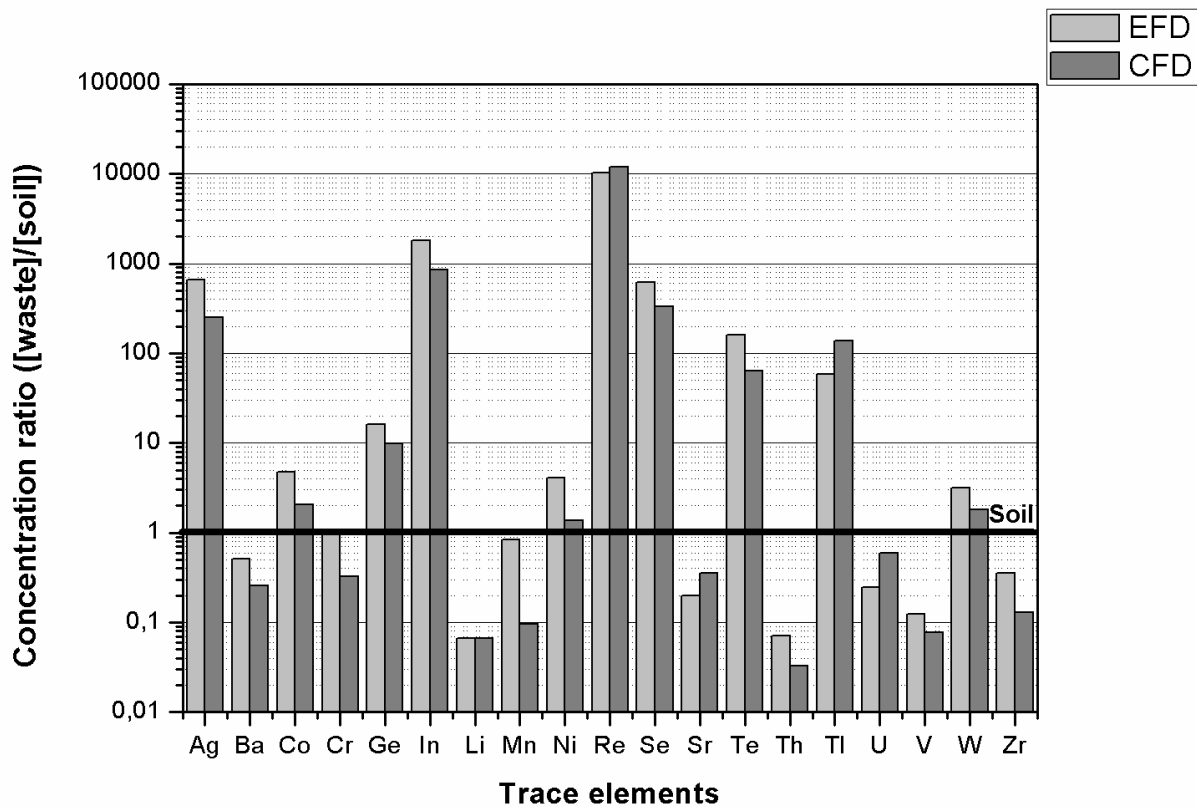


Figure 7. Comparison of the levels of trace elements in relation to estimated levels for global undisturbed soil composition

3.4 Thermogravimetric analysis

The samples were subjected to TGA, and the released gases were analysed using ICP-MS. The results are shown in Figures 8 and 9.

The EFD presents five thermal events, which take place at temperatures of 134°C, 510°C, 600°C, 834°C, and above 900°C. Water is detected in the first event, and this water is likely to come from crystallised water (Figure 8). Since this first peak is very wide, it is probable that hydroxide decomposition takes place between 300°C–500°C. More specifically, sodium hydroxide decomposition takes place in this temperature range [18].



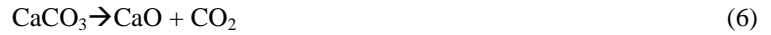
This compound is added in excess to the WTP to adjust the pH of the entering stream, whereby EFD is generated. The EFD has a sodium concentration of 0.26% which corresponds to 0.45% sodium hydroxide, calculated based on the stoichiometric reaction. Therefore, the decomposition of sodium hydroxide generates a loss of mass of 4.1%. The main loss of mass of this peak is likely to be due to the evaporation of crystallised water. At 510°C, CO₂ is released, and the decomposition of carbonates takes place. In this case, the decomposition of lead carbonate takes place [19]. It is estimated that sample contains about 8.5% of PbCO₃, approximately in agreement with the Pb concentration measured using FRX analysis.



SO₂ is released in the third event at about 600°C, and this probably comes from the decomposition of iron (II) sulphate (FeSO₄) which takes place at this temperature; this can mostly be found in various states of hydration [20]. This indicates the existence of water of crystallisation at 134°C (Eqs. 4 and 5). According to the proportion of mass loss, it is estimated that the sample contains less than 1% of this compound. However, the Fe contained in the sample is much higher, meaning that iron is joined with other elements.



Further loss of mass associated with the release of CO_2 occurs at 834°C . In this case, calcium carbonate (CaCO_3) is decomposed [21]; it has been calculated from the mass loss that the EFD contains around 3.5% of this substance.



The final thermal event takes place at a temperature of above 900°C ; SO_2 gases are detected again, which are probably due to the decomposition of calcium sulphate [19].

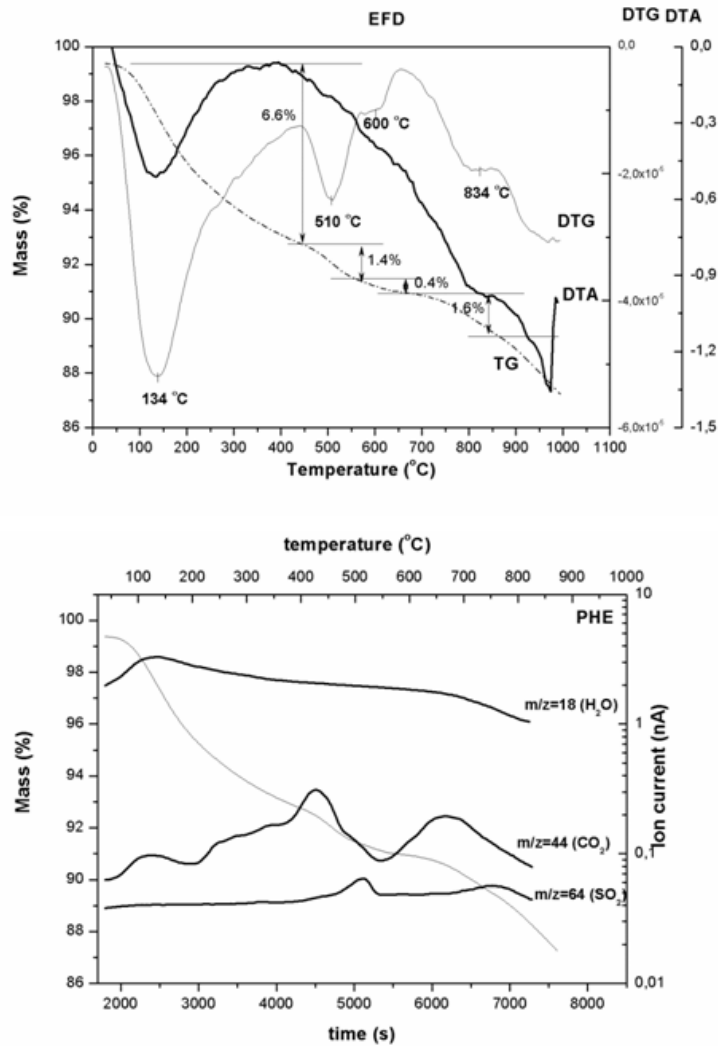


Figure 8. TG-DTG-DTA curve and gases detected in the EFD

The CFD presents four thermal events at 132°C , 453°C , 703°C and above 900°C . As can be observed in Figure 9, water is released at 132°C and 453°C in the same way as for the EFD. The first event is associated with the evaporation of crystallised water from a hydrated compound, and the second is due to the decomposition of hydroxides. In this case, calcium hydroxide decomposition takes place at this temperature [22]. This chemical species is added into the ceramic filter and a proportion remains unreacted. It was also identified using DRX analysis.



CO₂ was detected at 703°C, and this is associated with calcium carbonate decomposition [21]. This is in agreement with the DRX analysis (Eq. 6). Taking into account the mass loss obtained in the TG curve, the concentration of both compounds in the sample can be calculated. The CFD contains 26% Ca(OH)₂ and 10% CaCO₃. However, the proportion of Ca is somewhat lower than that obtained by FRX, and another compound of calcium must therefore be present in the sample. Previous studies [23, 24] suggest that a fraction of the calcium added into the gas stream of the ceramic filter reacts with the SO₂ gases, generating calcium sulphate (CaSO₄), which is decomposed above 900°C (Eq. 7) [19]. The DTA curve reveals that all events coming from the decomposition of chemical species contained in the CFD are endothermic.

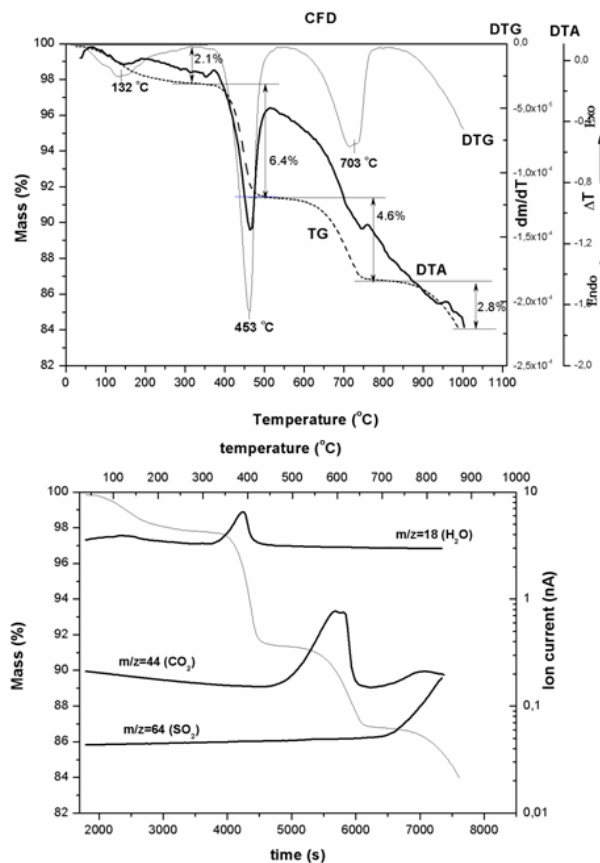


Figure 9. TG-DTG-DTA curve and gases detected in the CFD

3.5 Scanning electron microscopy

Figure 10 shows an agglomerated morphology for the EFD, with fine particles forming aggregates, although large particles are also present in the sample. This is in agreement with the granulometric analysis, which indicates two main particle distribution sizes. Based on this fact, it can be seen that the fine particles (point 2, Fig. 10) have high concentrations of Zn, Fe, Pb, Si, Cu, and As, which correspond to the main composition as measured using FRX analysis. Due to their amorphous morphology, it is impossible to differentiate the compounds that are present in the fine fraction. However, the large particles (point 1, Fig. 10) have high concentrations of Fe and Si according to the EDS spectra. Their composition and morphology, in form of smooth sheets, suggest that these particles are iron silicate (fayalite, Fe₂SiO₄) [25, 26]. The presence of fayalite is justified due to the water stream from slag granulation, which is composed of fayalite particles (Fe₂SiO₄); this is also managed in the WTP, where EFD is formed.

Fig. 11 shows a secondary electron image of an EFD region and the X-ray mapping for the elements S, Pb, Fe, As, Ca, Cu, Zn and Si present in the sample. This figure indicates that Pb, Fe, As, Cu, Zn and Si are uniformly distributed among the samples. Nevertheless, there are regions in which the presence of sulphur and calcium elements is coincident, confirming the existence of a CaSO₄ phase. At the same time, areas where iron and silicon are coincident can be observed, proving the existence of Fe₂SiO₄.

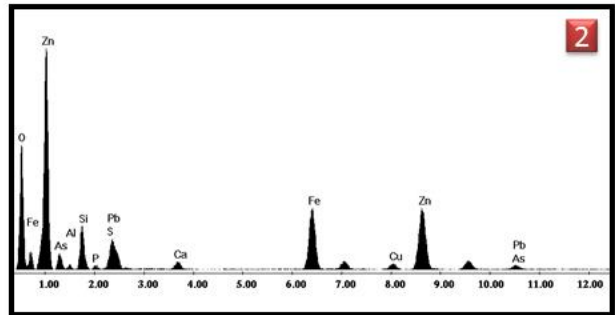
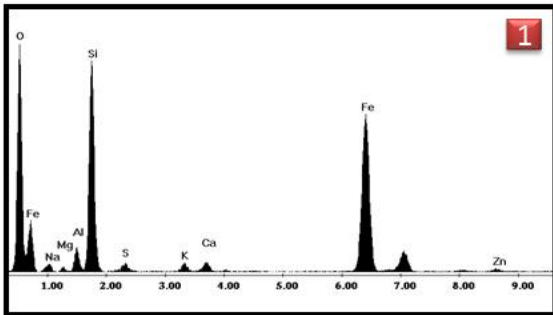
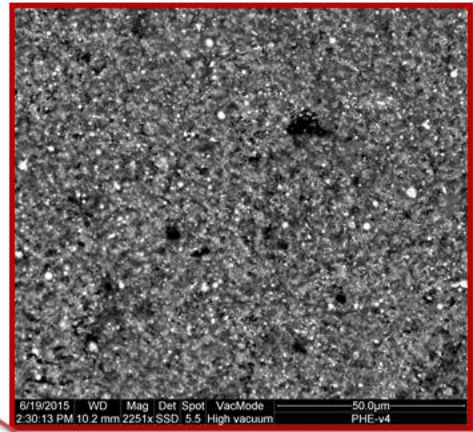
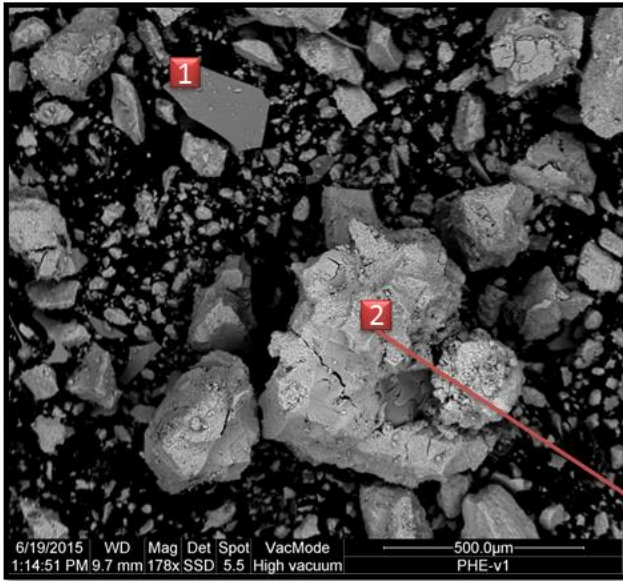


Figure 10. Scanning electron micrograph of EFD particles

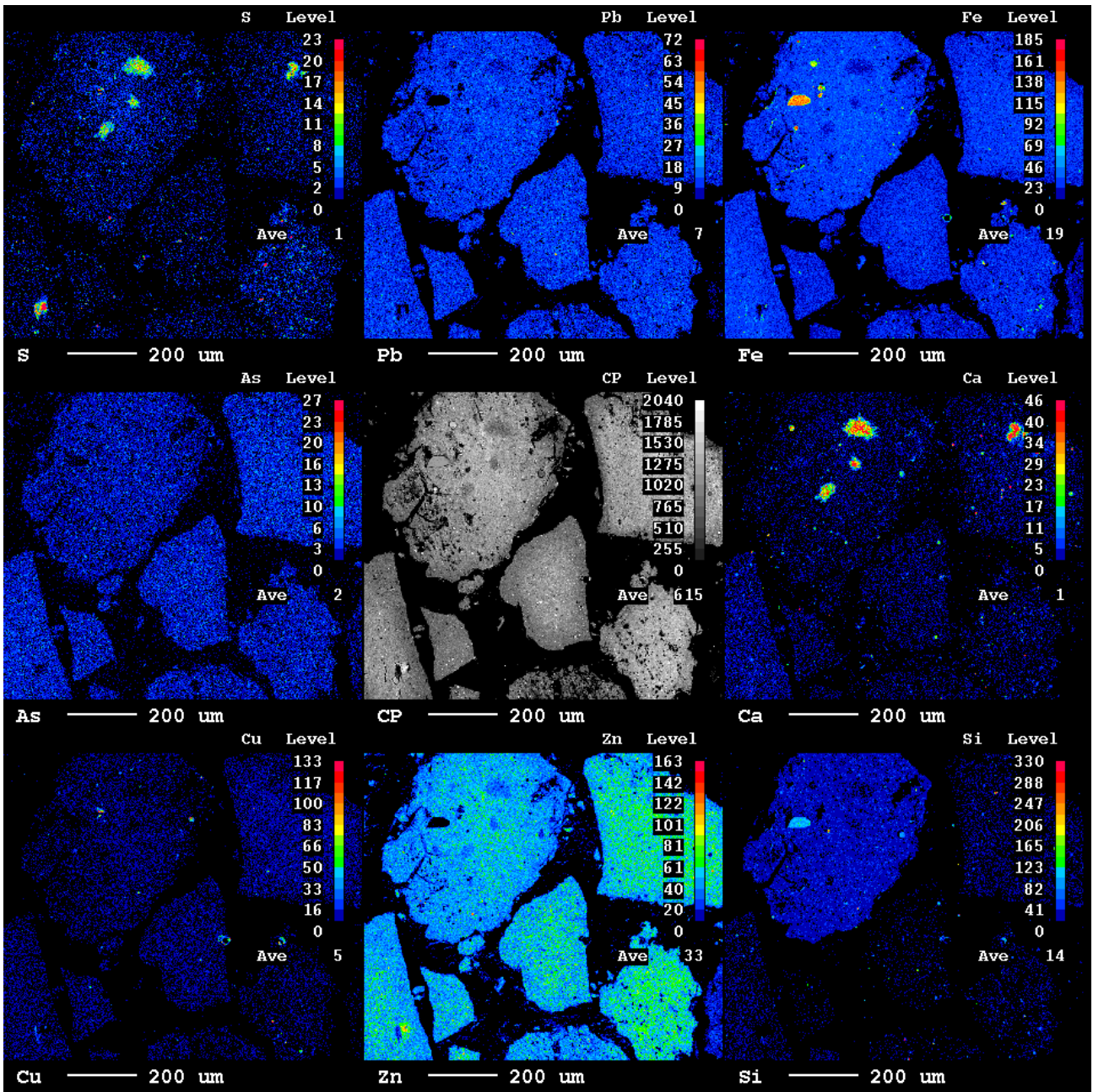


Figure 11. Secondary electron image of the EFD region, and distribution of S, Pb, Fe, As, Ca, Cu, Zn and Si

A general distribution of CFD particles is shown in Fig. 12, where it can be seen that the sample is characterised by three kinds of particles: a) large agglomerates of fine particles; b) intermediate; and c) very fine particles, fact in agreement with the laser grain-size analysis. According to the EDS results, the fine particles are composed of Zn, Ca, S, Pb, Si and Fe (point 4, Fig. 12), in agreement with the FRX results. These fine particles are characterised by their amorphous morphology, which makes the identification of compounds difficult. On the other hand, the intermediate particles (point 3, Fig. 12) contain a high proportion of calcium based on the EDS results. These particles therefore correspond to calcium hydroxide ($\text{Ca}(\text{OH})_2$), which is also identified using DRX and thermogravimetric analysis.

In this sense, a secondary electron image of the CFD region and X-ray mapping for several elements (S, Pb, Fe, As, Ca, Cu, Zn and Si) were carried out (Fig. 13). Pb, Fe, As, Cu, Zn and Si were distributed throughout the sample. However, there are regions in which the concentration of calcium is very high and others where the presence of sulphur and calcium are coincident, confirming that $\text{Ca}(\text{OH})_2$ and CaSO_4 are the main phases related to Ca.

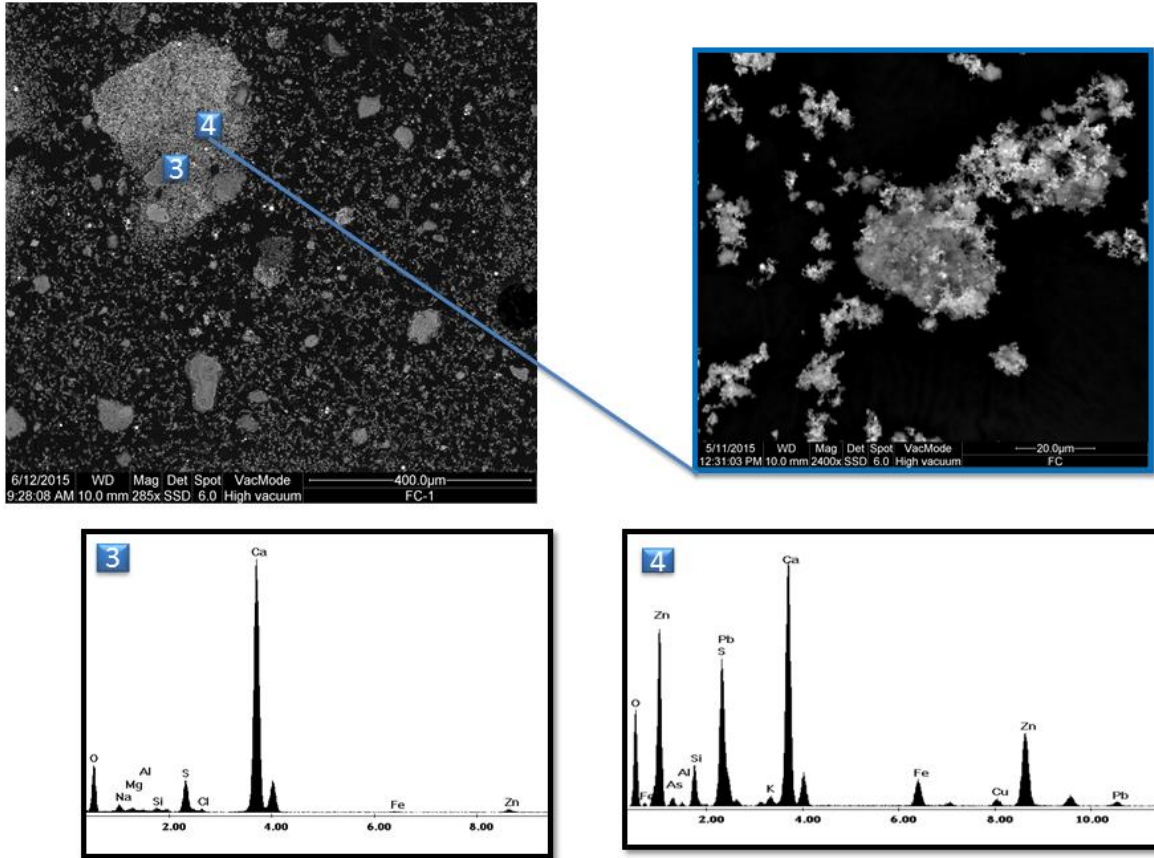


Figure 12. Scanning electron micrograph of CFD particles

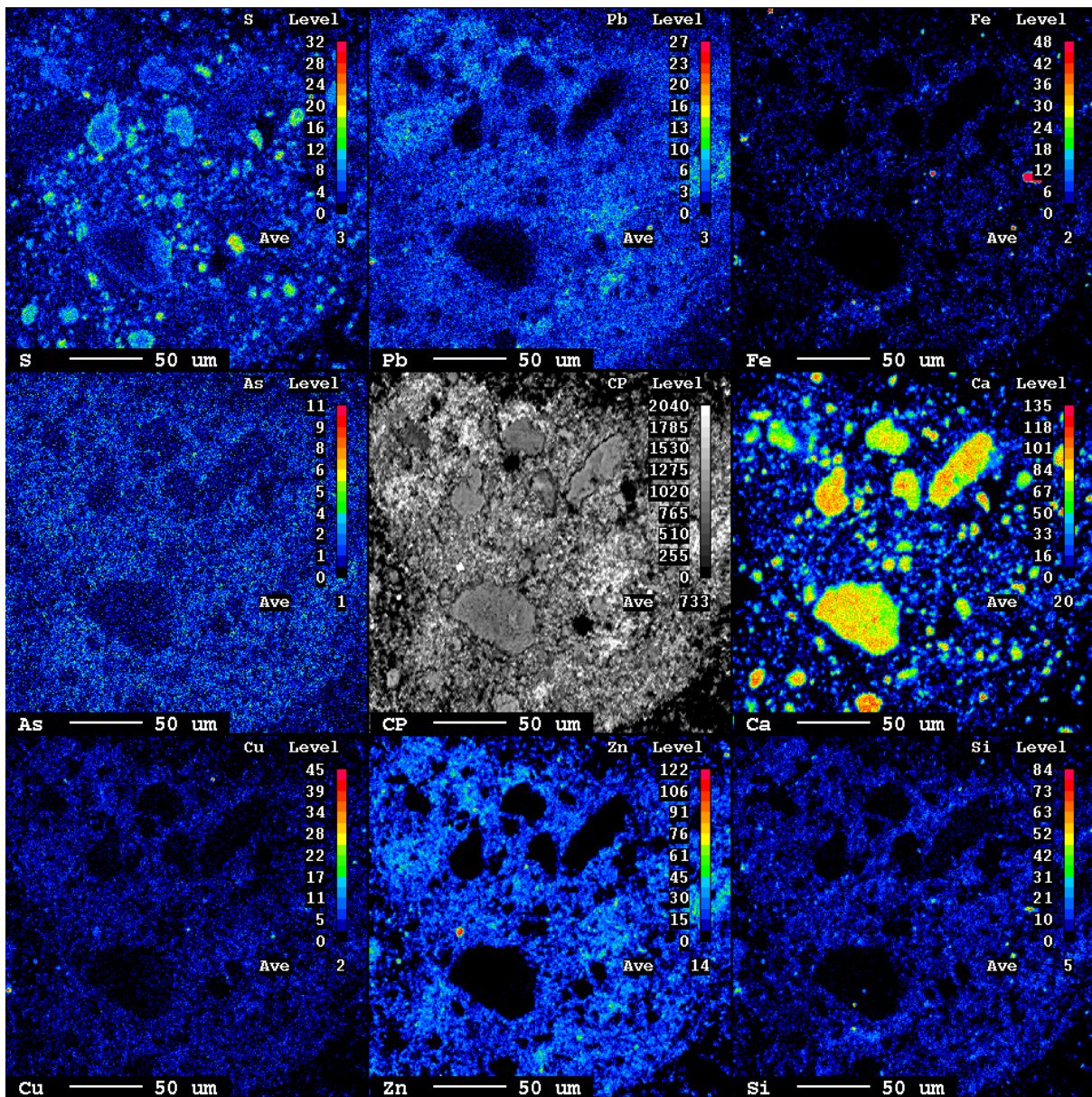


Figure 13. Secondary electron image of CFD region and distribution of S, Pb, Fe, As, Ca, Cu, Zn and Si

3.6 Lixiviation Test

The results of the TCLP tests and the limits of TCLP concentration for classification as hazardous waste are shown in Table 5. It can be observed that TCLP concentrations for Cd and Pb in the EFD are higher than the threshold (Cd: 1 mg/L; Pb: 5 mg/L); specifically, Cd exceeds the threshold value by 28 times and Pb by three times. However, the percentage of these elements leached is very low: less than 1.5% in case of Cd and less than 0.05% for Pb.

On the other hand, the CFD exceeds the established limits for Cd (Cd: 1mg/L) almost five times. Furthermore, the As and Pb values should be taken into account since these are very close to the TCLP limit (As: 5mg/L; Pb: 5mg/L). In the same way, the percentage of each element leached is low.

Element	Detection Limit (mg/L)	C _{EFD} (mg/L)	η (%)	C _{CFD} (mg/L)	η (%)	Threshold Level (mg/L)
Ag	0.005	<LD	-	<LD	-	5.0
Al	0.1	<LD	-	<LD	0.02	-
As	0.03	0.43 ± 0.09	0.002 ± 0.001	3.9 ± 2.1	0.03 ± 0.02	5.0
Ba	0.02	<LD	-	<LD	-	100
Bi	0.02	<LD	-	<LD	-	-
Ca	0.1	148 ± 2	2.6 ± 0.5	1378 ± 256	0.59 ± 0.17	-
Cd	0.002	28 ± 4	1.15 ± 0.32	4.6 ± 1.9	0.31 ± 0.15	1.0
Co	0.002	0.17 ± 0.01	0.24 ± 0.03	0.03 ± 0.01	0.10 ± 0.04	-
Cr	0.02	<LD	-	<LD	-	5.0
Cu	0.002	20 ± 1	0.05 ± 0.01	18 ± 10	0.10 ± 0.07	-
Fe	0.01	0.35 ± 0.06	(2.5 ± 0.8)·10 ⁻⁴	<LD	-	-
K	0.1	24 ± 5	2.4 ± 0.9	174 ± 61	3.6 ± 2.2	-
Mg	0.1	63 ± 4	2.2 ± 0.3	5.1 ± 1.6	0.32 ± 0.12	-
Mn	0.01	3.51 ± 0.12	0.54 ± 0.06	0.05 ± 0.02	0.06 ± 0.02	-
Mo	0.005	<LD	-	0.028 ± 0.16	0.03 ± 0.02	-
Na	0.1	173 ± 56	6.7 ± 2.4	39 ± 11	2.3 ± 0.8	-
Ni	0.005	<LD	-	LD	-	-
P	0.02	0.19 ± 0.07	0.008 ± 0.004	0.17 ± 0.08	0.03 ± 0.02	-
Pb	0.01	16 ± 1	0.02 ± 0.01	4.3 ± 0.80	0.01 ± 0.01	5.0
S	1	114 ± 3	2.7 ± 0.5	389 ± 34	0.79 ± 0.07	-
Sb	0.01	0.18 ± 0.03	0.003 ± 0.001	0.20 ± 0.07	0.01 ± 0.01	-
Se	0.02	<LD	-	<LD	-	1.0
Si	0.1	19.0 ± 1	0.08 ± 0.01	5.1 ± 2.1	0.05 ± 0.03	-
Sr	0.01	0.42 ± 0.04	0.66 ± 0.23	0.70 ± 0.23	0.62 ± 0.23	-
Te	0.01	0.09 ± 0.03	2.1 ± 1.0	<LD	-	-
Tl	0.01	0.29 ± 0.02	0.94 ± 0.17	0.52 ± 0.19	10.72 ± 0.31	-
U	0.05	<LD	-	LD	-	-
Zn		2340 ± 27	0.57 ± 0.01	553 ± 217	0.24 ± 0.15	-

Table 5. Results of the TCLP tests on the samples (USEPA method 1311). *C* = element concentration in the leaching liquid; *η* = transfer coefficient = fraction of the problem element in the solid transferred into the extracting liquid.

Furthermore, the results of the UNE tests and the reference limit value for non-hazardous materials are shown in Table 6. It can be seen that the UNE test concentrations for As and Cd in the EFD are higher than the UNE limits (As: 2mg/kg; Cd: 1mg/kg); specifically, the As concentration exceeds the value given by two times, and the Cd concentration is slightly higher. It is notable that potassium, sodium and sulphur are highly leached (K = 50%; Na= 100% and S=80%); however, these are below the reference limit values.

On the other hand, the CFD exceeds the established limits for As (two times higher), Cd (slightly higher), Mo (two times higher), Pb (seven times higher), and Zn (1.5 times higher) (As: 2 mg/kg; Cd: 1mg/kg; Mo: 10mg/kg; Pb: 10mg/kg; Zn: 50mg/kg). In the same way, potassium, sodium and sulphur are highly leached (K = 100%; Na= 72% and S=14%), but do not exceed the reference limit values.

Both test results confirm that the wastes are susceptible to generating leachates with high concentrations of pollutants which could be harmful to human health and the environment. Due to this fact, these wastes are currently subjected to an inertisation process before their disposal in a hazardous waste landfill.

Element	Detection Limit (mg/L)	C _{EFD} (mg/L)	η (%)	C _{CFD} (mg/L)	η (%)	Threshold Level (mg/L)
Al	0.1	<LD	-	<LD	-	-
As	0.03	3.9 ± 2.1	0.01 ± 0.01	2.0 ± 0.4	0.016 ± 0.003	2
Ba	0.02	0.40 ± 0.04	0.13 ± 0.02	<LD	-	100
Ca	0.1	1380 ± 500	24 ± 10	14700 ± 700	6.3 ± 0.7	-
Cd	0.002	1.04 ± 0.68	0.04 ± 0.02	1.35 ± 0.07	0.09 ± 0.01	1
Co	0.002	<LD	-	<LD	-	-
Cr	0.02	<LD	-	<LD	-	10
Cu	0.002	35 ± 22	0.10 ± 0.06	6.6 ± 0.3	0.037 ± 0.003	50
Fe	0.01	1.93 ± 1.89	0.001 ± 0.001	1.6 ± 0.3	0.006 ± 0.001	-
K	0.1	502 ± 146	50 ± 17	5450 ± 270	114 ± 29	-
Mg	0.1	560 ± 197	19 ± 7	<LD	-	-
Mn	0.01	0.35 ± 0.05	0.05 ± 0.01	<LD	-	-
Mo	0.005	2.7 ± 0.6	0.16 ± 0.04	18 ± 1	1.8 ± 0.2	10
Na	0.1	3382 ± 1300	130 ± 49	1220 ± 60	72 ± 6	-
Ni	0.005	3.3 ± 2.2	2.4 ± 1.6	<LD	-	10
P	0.02	1.7 ± 0.3	0.07 ± 0.01	0.6 ± 0.6	0.09 ± 0.09	-
Pb	0.01	1.8 ± 1.1	0.002 ± 0.001	68 ± 3	0.15 ± 0.04	10
S	1	3458 ± 1353	80 ± 34	6780 ± 339	14 ± 1	20000
Sb	0.01	0.40 ± 0.17	0.007 ± 0.003	<LD	-	0.7
Se	0.02	<LD	-	<LD	-	0.5
Si	0.1	22 ± 6	0.09 ± 0.03	<LD	-	-
Sr	0.01	3.7 ± 1.1	5.7 ± 2.1	2.9 ± 0.6	2.5 ± 0.5	-
Te	0.01	<LD	-	<LD	-	-
Tl	0.01	2.4 ± 0.7	7.8 ± 2.3	11.6 ± 5.8	16 ± 8	-
U	0.05	<LD	-	<LD	-	-
Zn	0.005	24 ± 16	0.006 ± 0.004	78 ± 4	0.04 ± 0.01	50

Table 6. Results of the UNE tests on the samples (UNE-12457-4). C = element concentration in the leaching liquid; η = transfer coefficient = fraction of the problem element in the solid transferred into the extracting liquid.

3.7 Diagnose for valorization

Both samples contain high proportion of Zn and Pb, so the recovery of these metal is considered the most appropriated potential route of valorization. There are different industrial processes dedicated to the recovery of Zn and Pb, but the dominant process is the Waelz rotary kiln. The process consists of treating zinc and lead containing material together with a carbon containing reductant, within a rotary kiln at 1000 °C to 1200 °C. The chemical process involves the reduction of zinc and lead compounds to elemental zinc and lead which volatilise and oxidise in the vapour phase to zinc and lead oxide. The zinc and lead oxide (Waelz oxide: 54-60% Zn, 7-10% Pb) is a feed product for zinc and lead smelters.

4. Conclusions

The present work is focused on the physico-chemical characterisation of two wastes, EFD and CFD, generated in the two desulphurisation treatments from EAF off-gases in order to determine basic information as an essential step towards finding applications or treatments for these wastes.

For EFD, the results show that:

1. It is mainly composed of Zn (41.4%), Fe (14.1%) and Pb (7.12%).
2. It has a high amorphous fraction (60%) and the crystalline fraction consists of zincite (ZnO), magnetite (Fe₃O₄), ramsdellite (MnO), quartz (SiO₂) and cristobalite (SiO₂).
3. Thermogravimetric analysis shows that EFD also contains NaOH, PbCO₃, CaCO₃ and sulphates, which may contain FeSO₄·xH₂O and CaSO₄.
4. The micro-structural analysis shows that the sample consists of agglomerates of very fine particles and large particles of iron silicate (Fe₂SiO₄).
5. The leaching tests according to USEPA and UNE show that the leachate exceeds the established limit.

For CFD, the results show that:

1. It consists mainly of Ca (23.2%), Zn (22.3%) and Pb (4.45%).

2. It has a high amorphous fraction (70%), and the crystalline fraction is made up of portlandite (Ca(OH)_2), zincite (ZnO), anglesite (PbSO_4), magnetite (Fe_3O_4), calcite (CaCO_3) and goethite (FeO(OH)).
3. Thermogravimetric analysis reveals the presence of calcium sulphate (CaSO_4). Micro-structural analysis shows that the sample consists of agglomerates of very fine particles.
4. The leaching tests according to USEPA and UNE show that the leachate exceeds the established limit.

Both desulphurisation treatments of the EAF off-gases generate wastes which are currently inertised before their disposal in landfill. However, a more interesting option from an environmental and economic point of view would be the recovery of Zn and Pb, due to the high content of these in the wastes.

Acknowledgments

This research has been supported by Atlantic Copper company project “Characterization of wastes from copper smelting and evaluation of potential applications”.

4. References

- [1] Doebrich J., 2009. Copper—A Metal for the Ages: U.S, Geological Survey,
- [2] Seetharaman S., McLean A., Guthri R., 2014. Chapter 2.1 – Copper Production, Treatise Process Metall. 534-624.
- [3] Raposeiras A.C., Vargas-Cerón A., Movilla-Quesada D., Castro-Fresno D., 2016. Effect of copper slag addition on mechanical behavior of asphalt mixes containing reclaimed asphalt pavement, *Constr. Build. Mater.* 119, 268–276.
- [4] Prasad P.S., Ramana G.V., 2016. Feasibility study of copper slag as a structural fill in reinforced soil structures, *Geotext. Geomembranes* 44, 623–640.
- [5] U.S. Congress, 1988. Office of Technology Assessment. Copper: Technology and Competitiveness. Chapter 8: Environmental Aspects of Copper Production, OTA-E-367, Washington. DC: U.S. Government Printing Office.
- [6] Csavina J., Taylor M. P., Félix O., Rine K. P., Sáez A. E., Betterton E. A., 2014. Size-resolved dust and aerosol contaminants associated with copper and lead smelting emissions: Implications for emission management and human health, *Sci. Total Environ* 493, 750–756.
- [7] DIRECTIVE 2010/75/EU OF THE EUROPEAN PARLIAMENT AND OF THE COUNCIL on industrial emissions (integrated pollution prevention and control), 2010.
- [8] European Commission, 2014. Best Available Techniques (BAT) Reference Document for the Non-Ferrous Metals Industries. Final Draft.
- [9] Montenegro V., Sano H., Fujisawa T., 2013. Recirculation of high arsenic content copper smelting dust to smelting and converting processes, *Miner. Eng.* 49, 184–189
- [10] Mineralogy Database, <http://www.webmineral.com/>, 2016 (accessed Sept 2016).
- [11] US Environmental Protection Agency, 1992. SW-846 Test Method 1311: Toxicity Characteristic Leaching Procedure.
- [12] UNE-EN 12457-4:2003 Caracterización de residuos. Lixiviación, Ensayo de conformidad para la lixiviación de residuos granulares y lodos, 2003.
- [13] Guézennec A., Huber J., Patisson F., Sessieq P., Birat J., Ablitzer D., 2005. Dust formation in Electric Arc Furnace: Birth of the particles, *Powder Technol.* 157, 2 – 11.
- [14] Machado J. G.M.S., Brehm F. A., Mendes Moraes C. A., Dos Santos C. A., Faria Vilela A. C., Marimon da Cunha J. B., 2006. Chemical, physical, structural and morphological characterization of the electric arc furnace dust, *J. Hazard. Mater.* B136, 953–960.
- [15] Li G. G., Keener T. C., Stein A. W., Khang S. J., 2000. CO_2 reaction with Ca(OH)_2 during SO_2 removal with convective pass sorbent injection and high temperature filtration. *Environ. Eng. Policy* 2, 47–56.
- [16] Rudnick R. L. and Gao S., 2003. Composition of the Continental Crust. University of Maryland, College Park, MD, USA.

- [17] Hu Z. and Gao S., 2008. Upper crustal abundances of trace elements: A revision and update, *Chem. Geol.* 253, 205–221.
- [18] Haynes W. M., 2015. *CRC Handbook of Chemistry and Physics*, 96th Edition.
- [19] Földvári M., 2011. Handbook of thermogravimetric system of minerals and its use in geological practice, Geological Institute of Hungary (Magyar Állami Földtani Intézet), 213.
- [20] Siriwardane R.V., Poston J. A., Fisher E. P., Shen M., Miltz A. L., 1999. Decomposition of the sulfates of copper, iron (II), iron (III), nickel, and zinc: XPS, SEM, DRIFTS, XRD, and TGA study, *Appl. Surf. Sci.* 152, 219–236.
- [21] L'vov B. V., 2002. Mechanism and kinetics of thermal decomposition of carbonates, *Thermochim. Acta*, 386, 1–16.
- [22] Gabrovšek R., Vuk T., Kaučič V., 2006. Evaluation of the Hydration of Portland Cement Containing Various Carbonates. *Acta Chim. Slov.*, 53, 159–165.
- [23] Fernández I., Garea A. and Irabien A., 1998. SO₂ reaction with Ca(OH)₂ at medium temperatures (300–425°C): Kinetic behavior, *Chem. Eng. Sci.*, 53, 1869–1881.
- [24] Chang J., Tian H., Jiang J., Zhang C., Guo Q., 2016. Simulation and experimental study on the desulfurization for smelter off-gas using a recycling Ca-based desulfurizer, *Chem. Eng. J.* 291, 225–237.
- [25] Fan Y., Shibata E., Iizuka A. and Nakamura T., 2014. Crystallization Behaviors of Copper Smelter Slag Studied Using Time-Temperature-Transformation Diagram, *Mater. T.*, 55, 958–963.
- [26] Potysz A., Kierczak J., Fuchs Y., Grybos M., Guibaud G., Lens P.N.L., Van Hullebusch E. D., 2016. Characterization and pH-dependent leaching behavior of historical and modern copper slags. *J. Geochem. Explor.* 160, 1–15.